ACS APPLIED MATERIALS & INTERFACES

Research Article

www.acsami.org

Collagen-Templated Bioactive Titanium Dioxide Porous Networks for Drug Delivery

William A. McMaster,[†] Xiaojian Wang,[‡] and Rachel A. Caruso*[,†,‡]

[†]Particulate Fluids Processing Centre, School of Chemistry, The University of Melbourne, Melbourne VIC 3010, Australia

[‡]CSIRO Materials Science and Engineering, Private Bag 33, Clayton South VIC 3169, Australia

Supporting Information

ABSTRACT: A Type I collagen gel was used as a template for fabricating porous titanium dioxide networks. Conducting sol–gel chemistry within the template, followed by a mild solvothermal treatment (selected TiO_2–collagen hybrids only), and then calcination to remove the template, produced anatase TiO_2 porous networks composed of mesoporous fibers. The collagen morphology was retained. TiO_2 fibers had walls up to 300 nm in thickness and hollow cores where the template was removed. Crystallite size, specific surface area (12.3–110 m^2 g^{-1}), mesopore diameter (4.2–8.8 nm), and pore volume of the networks varied under different synthesis conditions; solvothermal treatment of the hybrid doubled the surface area and mesopore diameter of the final material. Biomineralization was studied by immersion in a simulated body fluid. All networks displayed in vitro bioactivity, and hence potential bone-bonding capability, with apatite clusters growing on the fibers. Drug delivery was assessed by the adsorption and release of anti-inflammatory ibuprofen. Ibuprofen was stored both at the fiber surface and in mesopores below 15 nm in diameter, while release was a sustained diffusion process. The network solvothermally treated as a hybrid adsorbed ibuprofen up to 58.9 mg g^{-1}. The TiO_2 networks compared favorably with literature drug delivery vehicles when ibuprofen loading was normalized against surface area. Therefore, porous TiO_2 networks have potential as materials for biomedical applications.

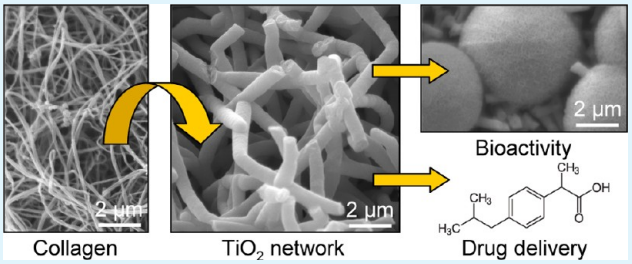

KEYWORDS: *biomineralization, collagen, porous, solvothermal, templating, titanium dioxide*

INTRODUCTION

Porous materials can be prepared by sol–gel chemistry and the templating technique.[1−15] For more than a decade, biomolecules such as alginate,[2] agarose,[4] cellulose and derivatives,[3−8,11] DNA,[6−8] organogelators[3,6−8] and cholesterol derivatives,[3,10] the tobacco mosaic virus,[3,6,7] and collagen[4−11] have been exploited as templates, often combined with liquid metal oxide precursors. Such is the versatility of the sol–gel/templating technique that beads,[1−3,15] fibers,[3,6,7,13] or networks of TiO_2,[3,4,13] as examples, can all be fabricated this way. Collagen is a popular template for synthesizing either porous, nanostructured metal oxides,[5−10] or biocomposites with hydroxyapatite (HAp) or metal oxides,[5,11,16−24] because collagen is a naturally occurring protein in mammals. There are 28 known types of collagen, of which seven form fibrils, while a further nine form fibril-associated collagens with interrupted triple helices. The most common, Type I collagen, is a fibril-forming collagen found in diverse body components such as skin or hide, bone, tendon, tooth, and nail.[6−9,16−18,22,23,25] Collagen fibers, usually of diameter 50–500 nm, form the extracellular matrix that serves as a scaffold for connective tissues, including bone.[16−18,24−29] The basic unit of collagen fiber, the collagen molecule, is a rodlike, right-handed triple-helix approximately 300 nm long and 1.5 nm in diameter, which is composed of three type II polyproline chains (PPII). Each PPII is comprised of a multiply repeated three-unit amino acid sequence. Consequently, collagen fibers are rich in surface functional groups (–OH, –COOH, $–NH_2$) that can participate in the templating of metal oxides.[6−11,17−19,23,25,26] Syntheses employing collagen solutions, fibers and gels have been reported for Al_2O_3,[7] SiO_2,[5,10,11] TiO_2,[6,7,17] and ZrO_2.[7−9] For example, Baia et al. created collagen-TiO_2 aerogel biocomposites. The collagen matrix was described as having a sponge-like structure, and this feature was carried over to the biocomposite.[17] In a series of papers, Liao and Shi and co-workers have utilized collagen fibers as templates for hierarchical, mesoporous metal oxide fibers.[6−9] In all syntheses, collagen fiber was mixed into a metal oxide precursor solution for standard sol–gel chemistry and templating; the template was removed by calcination.

There is considerable research interest in employing ordered microporous and mesoporous materials as drug delivery vehicles (DDVs).[30−46] These materials are characteristically chemically homogeneous, of high surface area and large pore volume, possessing well-defined, interconnected pores capable of hosting drug molecules, and have a surface that may be functionalized for further control over drug loading and release.

Received: June 19, 2012
Accepted: August 23, 2012
Published: September 5, 2012

   dx.doi.org/10.1021/am301093k | ACS Appl. Mater. Interfaces 2012, 4, 4717–4725

TiO_2 is both environmentally friendly and biocompatible, exhibiting little or no toxicity in vitro and in vivo.[1,6,28,47−50] Those properties indicate good potential as a biomaterial, for example as DDVs[30−32,48−50] or coatings for metallic implants.[28,31,47,51−53] For biomaterials, specific regard must be given to the surface chemistry and how it interacts with tissues.[54] A number of metal oxides and calcium-based bioceramics chemically bond to living bone through inducing the nucleation and growth of an intermediary bioactive apatite layer, a process known as biomineralization.[21,28,52−64] The same effect—surface formation of apatite—is evident when immersed in a simulated body fluid (SBF).[52,56−61] Hence, there are good prospects for a TiO_2-based biomaterial that provides a combination of local drug delivery and bioactivity (direct bone-bonding capability) to be used for biomedical applications, for example, in the treatment and regeneration of bone defects caused by bone cancers, as has started to be explored with SiO_2-based biomaterials.[35,46]

Therefore, in this manuscript a synthesis for collagen-templated, bioactive anatase TiO_2 porous networks composed of mesoporous fibers, that have potential as DDVs is reported. The open nature of the TiO_2 network, which was derived from the open network collagen template, could provide enhanced dispersion of drug molecules in vivo. For better exploring the bioactivity and DDV capability, it was desirable for the TiO_2 networks to cover a wide surface area range. However, with the sol−gel/templating technique, it can be difficult to produce materials that simultaneously retain a complex morphology, are mesoporous, highly crystalline, and have a high surface area. To overcome this difficulty, a postsynthetic solvothermal treatment was applied, as used previously by Chen et al.[15] Solvothermal treatment of TiO_2-collagen hybrids and short calcination time were key in achieving concurrent high surface area and high crystallinity for the networks. The favorable surface chemistry of anatase induced biomineralization. Scaffold architecture, especially high surface area, influenced the adsorption and release of ibuprofen from the mesoporous fibers of the TiO_2 networks.

EXPERIMENTAL SECTION

Materials. For preparation of the collagen gel template, pepsinated Apcoll-S purified soluble Type I collagen (approximately 3.0−3.2 mg mL^{-1}) from Devro Pty. Ltd. (Bathurst, NSW 2795, Australia) was used, along with Dulbecco's modified eagle's medium (DMEM) low glucose, with 1000 mg L^{-1} glucose, and sodium bicarbonate, without L-glutamine, liquid, sterile-filtered, cell culture tested from Sigma (product no. D5546), glacial acetic acid from Ajax, and sodium hydroxide pellets (GR) from Merck. The TiO_2 precursor, titanium-(IV) isopropoxide (97%, TIP) was supplied by Aldrich. Ethanol (AR) and isopropanol (AR) were both obtained from Chem-Supply. For apatite deposition from an SBF, the following reagents were employed: calcium chloride (anhydrous, Reag. Ph Eur) and sodium chloride (p.a.) from Merck; magnesium chloride hexahydrate (AR) and potassium chloride (AR) from Chem-Supply; dipotassium hydrogen phosphate (anhydrous, AR) and disodium carbonate (anhydrous, AR) from Ajax Finechem; sodium hydrogen carbonate (AnalaR) and sodium sulfate (anhydrous, AnalaR) were from BDH; sodium hydroxide pellets; and HEPES free acid (2-[4-(2-hydroxyethyl)-1-piperazinyl]ethane sulfonic acid; high purity grade) from AMRESCO. For the ibuprofen study, ibuprofen (98%), and phosphate buffered saline (PBS), 10× concentrate (product no. P7059), were both purchased from Sigma-Aldrich; n-hexane (>98%) came from Merck. All chemicals were used as received. The water used in all experiments was passed through a Millipore Milli-Q ultrapure water purification system, and had a resistivity higher than 18.2 MΩ cm.

Synthesis. *Preparation of the Collagen Gel.* Collagen gel was prepared according to a literature method.[65] Soluble collagen was diluted with cold aqueous 0.1% acetic acid to 3.0 mg mL^{-1}, then combined in a container with DMEM in a ratio of 1:2, giving a collagen concentration of 1.0 mg mL^{-1}. NaOH (1.0 M) was then added in the ratio 2 μL/0.6 mL collagen-DMEM mixture. The solution was immediately gently mixed, the container covered with Parafilm M and the collagen allowed to gel overnight at room temperature (approximately 20 °C). The gelled collagen was removed from the container by inverting the container and allowing the gel to slide out. The gel was sliced with a scalpel into irregularly shaped pellets of about 1 cm^3, and solvent exchanged from water to ethanol, and finally to isopropanol.

Titanium dioxide fabrication. TiO_2 templating of the gel was effected using a reported method.[4] Collagen gel was soaked overnight (16 h) in 70 wt % TIP in isopropanol, and then the gel pieces were transferred to a water/isopropanol solution (1:1 volume) for hydrolysis and condensation reactions (6 h), after which the TiO_2-collagen hybrids were dried at room temperature for 2 days, followed by 6 h at 60 °C. A portion of the hybrids underwent solvothermal treatment (detailed below), then all samples were heated under flowing air at 450 °C in a muffle furnace (31165A B&L Tetlow with Shimaden FP21 controller) for either 2 or 10 h, employing a heating ramp from 25 to 450 °C of 3 K min^{-1}, in order to remove the collagen and crystallize the TiO_2. The calcination temperature had been determined by thermogravimetry (5 min isothermal period at 25 °C, followed by heating from 25 to 800 °C at 10 K min^{-1}) under oxygen (30 mL min^{-1}) as the temperature above which no further significant mass loss occurred. The final materials were designated No-10 h, No-2 h, and ST-2 h, where ST and No represent solvothermal treatment or no treatment, respectively, and the numeral is the calcination time.

Solvothermal Treatment. Solvothermal treatment of the TiO_2-collagen hybrids occurred prior to calcination, utilizing a literature method.[15] Pieces of hybrid (up to 1.6 g) were placed into Teflon-lined autoclaves (volume 50 mL) along with ethanol (20 mL) and water (10 mL), and then heated at 160 °C for 16 h. Once cooled the solid contents were collected on a Hirsh funnel with an Advantec filter paper (grade 2 qualitative filter paper) under vacuum, rinsed three times with ethanol, then dried in air for 2 days.

Characterization. Scanning electron microscopy (SEM) was performed on an FEI Quanta 200 environmental scanning electron microscope in order to study the morphology of the collagen gel (after CO_2 critical point drying (CPD) using a Bal-Tec critical point dryer), hybrids, final TiO_2 structure, and TiO_2-apatite biomaterial. All samples for SEM were sputter coated with gold. Nitrogen sorption data were obtained using a Micromeritics Tristar 3000 to determine both the Brunauer-Emmet-Teller (BET) surface area of the samples, as well as porosity according to the adsorption branch of the Barrett−Joyner−Halenda (BJH) model, including the single-point total pore volume calculated at $P/P_0 = 0.98$. Calcined samples were degassed overnight under vacuum (≤13 Pa) at 150 °C; samples applied in the ibuprofen study at 105 °C, and; CPD collagen gel and TiO_2−collagen gel hybrids at 25 °C. Thermogravimetric analysis (TGA) and single differential thermal analysis (SDTA) were conducted simultaneously on a Mettler Toledo TGA/SDTA851e instrument. Powder X-ray diffraction (XRD) patterns were acquired on a PANalytical X'Pert Pro Diffractometer using Cu Kα radiation and an X'Celerator detector employing real-time multiple strip detection. In preparation for XRD, samples were dried overnight at 110 °C then ground into powder. Energy dispersive X-ray spectroscopy (EDS) analysis of the SBF-derived apatite was carried out with an Oxford Instruments EDS detector attached to a Leica 440 scanning electron microscope. UV−visible spectroscopy for the ibuprofen study was carried out with a CARY 1E spectrophotometer (scanning range: 320−220 nm; rate: 600 nm min^{-1}).

Bioactivity Assessment. Modified simulated body fluid (m-SBF) for the deposition of bone-like apatite was prepared according to the method of Kim et al.[62] Into approximately 1.4 L of water were sequentially dissolved NaCl (10.8065 g), $NaHCO_3$ (1.0084 g), Na_2CO_3 (0.8523 g), KCl (0.4505 g), K_2HPO_4 (0.3512 g), $MgCl_2.6H_2O$ (0.6224 g), HEPES (35.7843 g) which was first

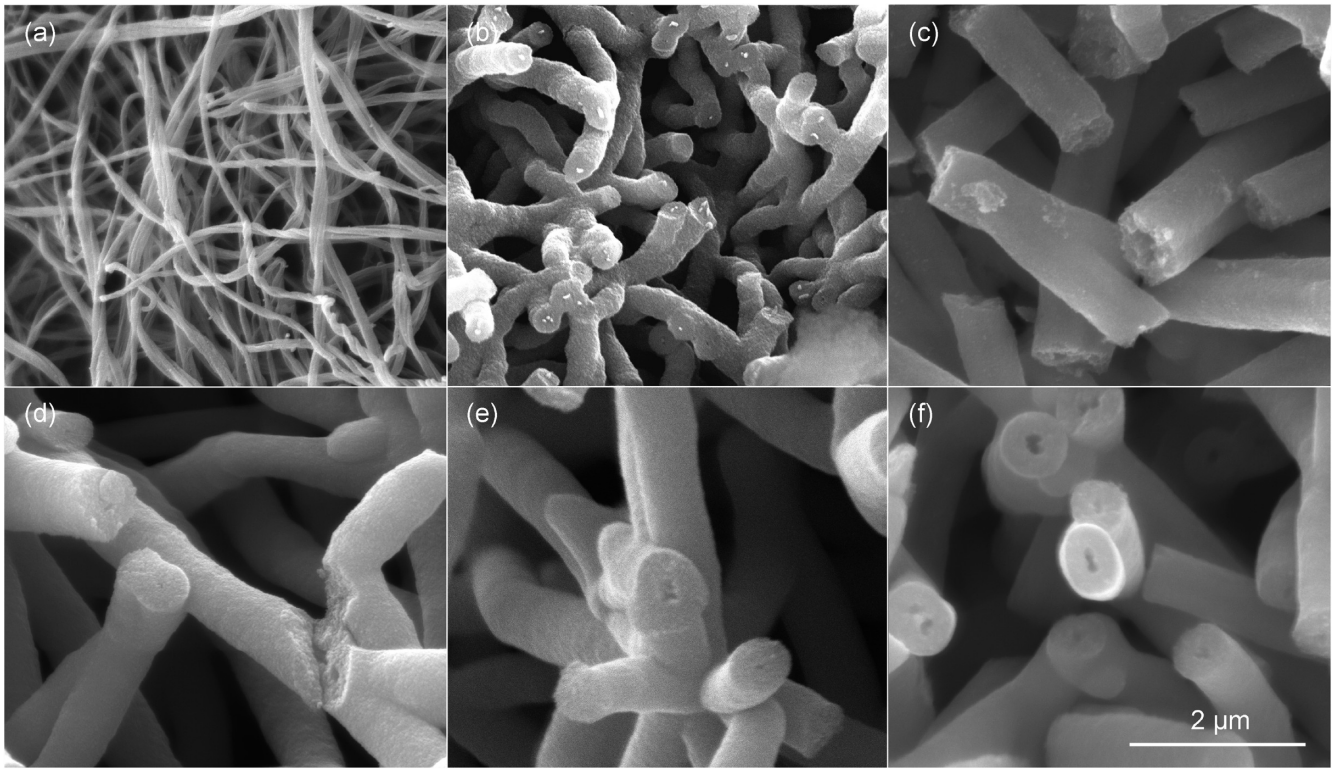

Figure 1. SEM images of (a) CPD collagen gel, (b) TiO_2–collagen hybrid before solvothermal treatment, and (c) afterward, (d) No-10 h, (e) No-2 h, and (f) ST-2 h. All images are at the same scale.

dissolved in 200 mL of 0.2 M NaOH, $CaCl_2$ (0.5865 g), and Na_2SO_4 (0.1441 g). Additions of NaOH (1.0 M) were made until the mixture reached pH 7.4. The solution was made to 2 L in a volumetric flask, and stored in a polyethylene bottle in the refrigerator.

Fifteen pellets of a TiO_2 network were divided between five polypropylene containers of volume 120 mL. The containers were filled to the 65 mL mark with SBF, had their lids loosely affixed, and were then placed in the incubator chamber of a digitally controlled Ratek Orbital Mixer Incubator OM11 set to 37 °C and 120 rpm. The SBF in the containers was completely drained and refilled every two days. A beaker containing 400 mL of water was also placed into the incubator in order to create a humid atmosphere and prevent rapid evaporation of the SBF. The TiO_2–apatite hybrids were removed from the SBF after 1, 3, 7, 14, and 21 days, placed momentarily on a KIMTECH Science Kimwipes wiper (Kimberly-Clark Professional) to wick up excess SBF, then dried in air at room temperature for 24 h. SEM was employed to assess the growth and coverage of the TiO_2 networks by apatite, EDS for surface elemental analysis, and nitrogen sorption for the effect on surface area and porosity.

Ibuprofen Adsorption and Release. The adsorption and release study of ibuprofen, as a model drug, followed a reported procedure.[40]

Adsorption. Ibuprofen was dissolved in hexane to a concentration of 30 mg mL^{-1}. To each solution (100 mL) was added 0.3 g of a TiO_2 network, which was previously ground to powder. This mixture was sealed in a container and slowly stirred for 30 min, before being put into an oven for 72 h at 37 °C. The ibuprofen-loaded TiO_2 powder was separated from solution by centrifugation (Eppendorf, 10,000 rpm), washed three times with hexane, then dried overnight in a vacuum oven at 60 °C. Control materials without ibuprofen were also prepared following the same procedure using hexane solutions without ibuprofen.

Release. Ibuprofen-loaded TiO_2 networks were compacted into discs (diameter 10 mm) under a pressure of 4 MPa. For release, the pellets were placed into 1× PBS (50 mL), prepared by diluting 10× PBS with water. Parallel in vitro experiments were performed. Aliquots (2 mL) were periodically taken from the free solution, and immediately replaced with the same volume of fresh PBS. The aliquot was diluted to 20 mL with PBS then analyzed by UV–vis spectroscopy at a wavelength of 264 nm. The concentration of drug present in the aliquot was determined from a calibration curve. Calculation of the corrected concentration for the ibuprofen released was achieved through the following equation[40]

$$C_{t\mathrm{corr}} = C_t + \frac{v}{V}\sum_{0}^{t-1} C_t \qquad (1)$$

Where $C_{t\mathrm{corr}}$ is the corrected concentration at time t, C_t is the measured concentration at t, v is the volume of the aliquot taken, and V is the volume of release medium. The release data (presented as means (n = 2) and standard deviations) were fitted to the Higuchi model, whereby drug release is a diffusion process governed by Fick's law in accordance with this equation[40]

$$Q = k_H t^{0.5} \qquad (2)$$

Where Q (mg g^{-1}) is the mass of drug released (relative to the mass of the TiO_2 network) at the square root of time t (h), and k_H is the Higuchi dissolution constant (mg g^{-1} $h^{-0.5}$), which can be determined from the slope of the linear portion of a plot of Q versus $t^{0.5}$.

RESULTS AND DISCUSSION

Characterization of the Template, Hybrids, and Final Materials. Collagen is a natural protein which exists in several different forms, with the most common being Type I.[17,25] The collagen gel utilized in this research was Type I, prepared from a commercial, pepsinated, solubilized collagen. The gelling process began immediately upon addition of NaOH to the collagen-cell culture medium mixture.[65] The final gel had a collagen content of 0.1 wt %, which formed an open network (see Figure S1a in the Supporting Information) comprising fibers 50–100 nm in diameter, consistent with the low end of the range of diameters for collagen fibers.[27,28] Templating of the collagen fibers with TiO_2 from a titanium alkoxide

precursor produced TiO_2 fibers; hydrogen bonding was considered to be the mechanism responsible for the collagen−TiO_2 interaction, because the collagen molecule has a wealth of applicable functional groups.[6−9,23] Finally, calcination of the TiO_2−collagen hybrids removed the organic template, creating an open network of interconnecting TiO_2 fibers (see Figure S1b in the Supporting Information). Across all final materials the overall network structure was consistent, as was observed at lower SEM magnifications. Fibers were separated by spaces of hundreds of nanometers to several micrometers. Each sample was observed to be both porous and structurally homogeneous throughout. SEM images of CPD collagen gel, TiO_2−collagen hybrid, and calcined TiO_2 networks are shown in Figure 1. Collagen fibrils, as a gel, have been reported to serve as a template for the structuring of SiO_2.[5,10] Despite different synthesis routes, SiO_2 fibers produced from gels by Ono et al.[10] and Eglin et al.[5] were alike, being roughly tubular, had internal diameters of approximately 50 nm,[10] and 50−100 nm,[5] respectively, and thin walls (estimated thickness 10−25 nm) of agglomerated SiO_2 particles. The walls of our TiO_2 fibers stand in marked contrast, being up to 300 nm in thickness. Yet in common with the SiO_2 fibers, the collagen morphology was evident, and was retained throughout the TiO_2 fiber synthesis. The final fibers, as well as solvothermally treated hybrids, exhibited roughly cylindrical hollows corresponding to the diameter and central location of the collagen fibers (compare Figure 1a with c−f), commensurate with collagen-templated SiO_2 fibers.

To investigate the TiO_2 structural evolution during calcination and solvothermal treatment, thermal analysis was employed. TGA indicated that pyrolysis of CPD collagen gel occurred above 190 °C (see Figure S2 in the Supporting Information). For the TiO_2−collagen hybrids, regardless of solvothermal treatment, no further significant mass decrease took place above 400 °C. Hence, sustained heating at 450 °C was employed in the calcination step. Mass losses for solvothermally treated hybrids were always markedly less than for nontreated hybrids, suggesting that much of the organic template had been removed during solvothermal treatment. This is supported by the presence of hollows within the solvothermally treated TiO_2−collagen hybrid fibers prior to calcination (see Figure 1c).

DTA of the solvothermally and nonsolvothermally treated hybrids showed distinct differences in the behavior of the hybrids when heated. For both samples, adsorbed water was removed before 150 °C; however, only the hybrid that did not experience solvothermal treatment had significant exothermic evolutions, with peaks around 300 and 400 °C (see Figure S2 in the Supporting Information). The former peak is associated with pyrolysis of the collagen template; the latter peak with crystallization of the inorganic material. The association of the peak at approximately 400 °C with crystallization was inferred from XRD patterns (see Figure 2). Initially the hybrid was XRD amorphous (Figure 2a), whereas after calcination anatase crystals were detected (Figure 2c, d). During solvothermal treatment, crystallization was induced (hence the 400 °C peak was absent in the DTA curve for the solvothermally treated hybrid), producing anatase (Figure 2b), which remained after calcination (Figure 2e).

Anatase crystal sizes were calculated by applying the Scherrer equation to the (101) peak (see Table 1). It was noted that the solvothermally treated sample after calcination had smaller crystal sizes than the networks that did not undergo treatment,

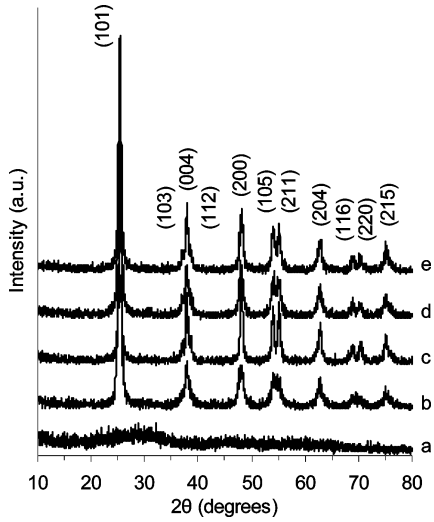

Figure 2. Typical XRD patterns of (a) TiO_2−collagen hybrids before solvothermal treatment and (b) afterward, and of the final networks (c) No-10 h, (d) No-2 h, and (e) ST-2 h.

Table 1. Crystal Size (D_{XRD}) Determined from the Anatase (101) Peak, BET Surface Area (S_{BET}), Mesopore Diameter at Maximum Pore Volume (D_P), and Single-Point Pore Volume (V_P) of the Samples

sample	D_{XRD} (nm)	S_{BET} ($m^2\ g^{-1}$)	D_P (nm)	V_P ($cm^3\ g^{-1}$)
CPD collagen gel	N/A	159 ± 1	66.4	0.868
hybrid	amorphous	504 ± 2	<2	0.283
treated hybrid	10.3	140 ± 1	8.9	0.315
No-10 h	20.8	12.3 ± 0.1	5.3	0.040
No-2 h	15.7	48.9 ± 0.4	4.2	0.074
ST-2 h	10.7	110 ± 1	8.8	0.251

and that longer heating time increased crystal size. Without solvothermal treatment, and after calcination for 10 h, crystal size (D_{XRD}) was 20.8 nm, reducing to 15.7 nm for only 2 h calcination; with the solvothermal step, D_{XRD} was just 10.7 nm. Lower surface area for longer calcination time correlates with the larger crystal sizes determined from powder XRD; reduction in surface areas from the hybrids to the calcined networks is attributable to temperature-induced growth of TiO_2 crystallites (Table 1). Thus, heating five times longer, as happened for No-10 h compared with No-2 h, produced final materials with BET surface areas (S_{BET}) of 12.3 and 48.9 $m^2\ g^{-1}$, respectively. The S_{BET} of ST-2 h was 110 $m^2\ g^{-1}$, more than double No-2 h. This dramatic increase in surface area was due to solvothermal treatment prior to calcination that resulted in small crystal size. It is known that for the hydrothermal treatment of amorphous TiO_2 gels at low and moderate temperatures (80 and 180 °C, respectively), a high water content favors the nucleation of nanocrystals, which will be of a small crystallite size (e.g., 6−10 nm), rather than rapid crystal growth.[12] Although water was the minor fraction of our solvothermal fluid, it was still present in a large excess compared to the amorphous TiO_2 component of the TiO_2−collagen hybrids. Consequently, D_{XRD} for the treated hybrid was only 10.3 nm (Table 1). During the subsequent calcination step, crystal growth was strongly retarded with the crystal size increasing by only 4% from the treated hybrid to ST-2 h.

To explore the porous structure, nitrogen sorption was conducted on the collagen, hybrid, and final materials. Nitrogen

sorption isotherms for the TiO_2 networks were classified as Type IV—mesoporous solid (see Figure S3a in the Supporting Information). The mesopore diameter was determined from the adsorption branch of the BJH model (the adsorption branch was chosen because of closer identification of the hysteresis loop as H2 type,[66] except for the CPD collagen gel where the desorption branch was used). Solvothermal treatment affected the mesopore diameter—pore diameter was doubled with treatment—and the total pore volume of the TiO_2 networks, while calcination time played a secondary role increasing the mesopore diameter, but reducing the total pore volume (see Table 1). These findings indicate that solvothermal treatment was key to high surface area, enhanced mesopore diameter, and high pore volume, whereas the thermally induced mesopore diameter increase came at the expense of pore volume.

Pore size distributions for the TiO_2 networks are presented in Figure 3. These mesopores were considered to represent the

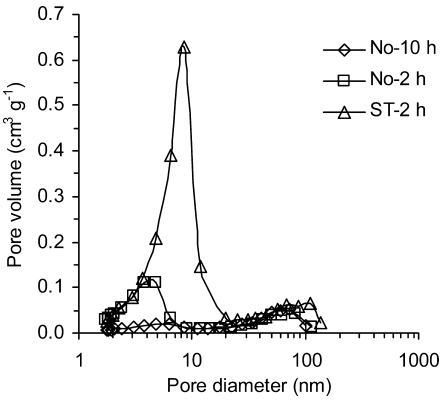

Figure 3. Nitrogen adsorption pore size distributions of the TiO_2 networks.

TiO_2 interparticulate space. Enlargement of mesopores in SiO_2 after hydrothermal treatment has been previously reported.[35] Ono et al. determined pores of 4 and 50 nm diameter in their SiO_2 fibers: The large pore diameter resulted from SiO_2 tube formation after burnout of collagen fibers, whereas the small pore diameter was credited to the hierarchical bundling of collagen fibers.[10] Literature concerning templated metal oxides using collagen has almost exclusively reported mesopores of less than 10 nm.[5−7,9,10] TiO_2 networks in the present work had both small interparticle mesopores, and larger mesopores and macropores that correlate to the removal of collagen fibers. This pore hierarchy was attributed to using a 0.1 wt % collagen gel as the template. Fabrication of a metal oxide network becomes uncertain when the gel concentration is high (e.g., 10 wt %),[5] and does not occur when the template takes the form of large bundles of aligned collagen fibers.[6−9]

Representing interfiber pores, pore volume pertaining to larger pores in the range of 30−100 nm was present in the CPD collagen gel and hybrids (see Figure S4 in the Supporting Information), and this was carried through to the final TiO_2 materials (Figure 3). A contribution to the macropore volume from the cylindrical hollows observed by SEM (Figure 1) was also expected; however, this cannot be identified separately to the interfiber pore volume.

In this section was presented the characterization of three open networks of interconnecting anatase TiO_2 fibers, where the fibers were mesoporous. Each network exhibited distinct differences in surface area, mesopore size, and pore volume (see Table 1). The following sections examine the effect of these textural properties on both biomineralization and drug delivery capability.

Bioactivity Assessment. The TiO_2 networks were immersed in m-SBF (see the Supporting Information) for up to 21 days. Mineral clusters formed on all three anatase phase TiO_2 networks. EDS was used to probe the elemental composition of these clusters, and a spectrum was obtained (see Figure S5 in the Supporting Information). The defining feature of an SBF is that the ions present (Na^+, K^+, Mg^{2+}, Ca^{2+}, Cl^-, HCO_3^-, HPO_4^{2-}, and SO_4^{2-}) match those found in blood plasma, and are at or near their physiological concentrations.[60,62] With the exception of potassium (and hydrogen—too light for detection), elements of all these ions were detected (see Figure S5 in the Supporting Information). Titanium was also detected and relates to the underlying TiO_2 network. According to the biomineralization mechanism, these minor ions are incorporated into the calcium phosphate when amorphous calcium phosphate (ACP) transforms to poorly crystalline, bone-like apatite,[52,58,59,61,67,68] although more recent work suggests that minor ion incorporation occurs soon after initial ACP formation.[55] The Ca/P peak ratio was 1.65 (see Figure S5 in the Supporting Information). For HAp, Ca/P is 1.67. Therefore, the formed mineral clusters were considered to be apatite. Irrespective of when the minor ions are incorporated into ACP/apatite, it is the inclusion of carbonate ions (capable of substituting for both $OH^-$and PO_4^{3-} in HAp) that makes apatite characteristically carbonated and calcium deficient.[55] The nucleation of apatite on the TiO_2 fibers was in agreement with the biomineralization mechanism. At physiological pH, TiO_2 in SBF has a net negative charge, the formation of which is key to epitaxial apatite nucleation. Apatite growth proceeds by repeated electrostatic interactions, through sequential attraction of Ca^{2+} and HPO_4^{2-} to form first ACP, which ultimately transforms into apatite.[28,52−61,63,67,68]

Nucleation and growth of apatite on a substrate are widely held to indicate that the substrate material is in vitro bioactive.[52,53,59−62,67,68] Apatite clusters grew on all three samples. Thus the networks were considered in vitro bioactive, and would be expected to bond to living bone if utilized in vivo. Interestingly, the apatite clusters were located almost exclusively on the outside of the network pellet. Cluster formation was well in evidence after 7 days (see Figure 4a−c), and considerable, if not total, over the outside of the pellet by 21 days (Figure 4d). Apatitic cluster development within the TiO_2 fiber network was uncommon, as observed by SEM (Figure 4e). Mature apatite growths typically appear as large spherical or hemispherical clusters comprised of innumerable wormlike plates (for example, as shown in Figure 4f), suggesting porosity. Occasionally the clusters were observed to have grown around one or more TiO_2 fibrils. The morphology of the clusters was consistent with other reported HEPES-buffered, SBF-derived apatite deposits.[29,63,67]

Nitrogen sorption was engaged to explore the effect of apatite formation and growth on the TiO_2 networks. For all networks, there was an immediate decrease in the volume of the primary mesopore after immersion in SBF for one day, with pore volume remaining reduced for the duration of the 21 days (see Figure S6 in the Supporting Information). Surface areas were consequently diminished. For No-10 h, the presence of apatite caused a very considerable loss of porosity for mesopores of less than 10 nm (see Figure S6a in the

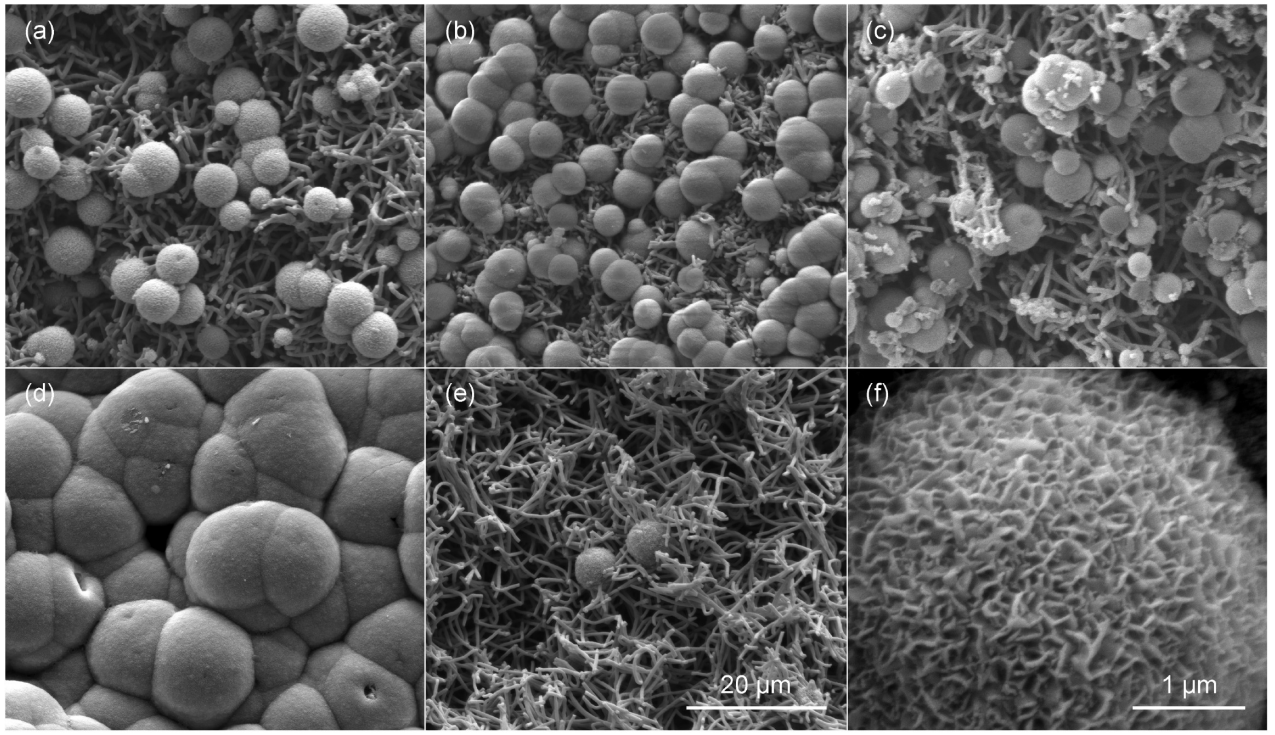

Figure 4. SEM images of (a–c) apatite clusters on No-10 h, No-2 h, and ST-2 h after 7 days in m-SBF; (d) coalesced apatite clusters have covered a TiO_2 network (No-2 h) after 21 days; (e) isolated and alone, a pair of apatite clusters inside of a No-10 h pellet at 21 days, and; (f) an apatite cluster at 14 days. Images a–e are all at the same scale.

Table 2. BET Surface Area (S_{BET}), Mesopore Diameter at Maximum Pore Volume (D_P), and Single-Point Pore Volume (V_P) of the Ground TiO_2 Networks, Both Before and After Ibuprofen Adsorption; the Mass of Ibuprofen Adsorbed as Determined by UV–vis, and the Higuchi Dissolution Constant (k_H)

	S_{BET} (m^2 g^{-1})		D_P (nm)		V_P (cm^3 g^{-1})			
network	before	after	before	after	before	after	ibuprofen (mg g^{-1})[a]	k_H (mg g^{-1} $h^{-0.5}$)
No-10 h	12.1 ± 0.1	8.6 ± 0.1	5.4	5.1	0.032	0.028	11.9 ± 2.0	0.789
No-2 h	45.1 ± 0.3	37.1 ± 0.4	4.3	3.9	0.065	0.056	30.8 ± 3.2	6.51
ST-2 h	102 ± 1	90 ± 1	8.7	8.7	0.238	0.206	58.9 ± 2.0	5.50

[a]The accumulated mass of ibuprofen released at t = 96 h.

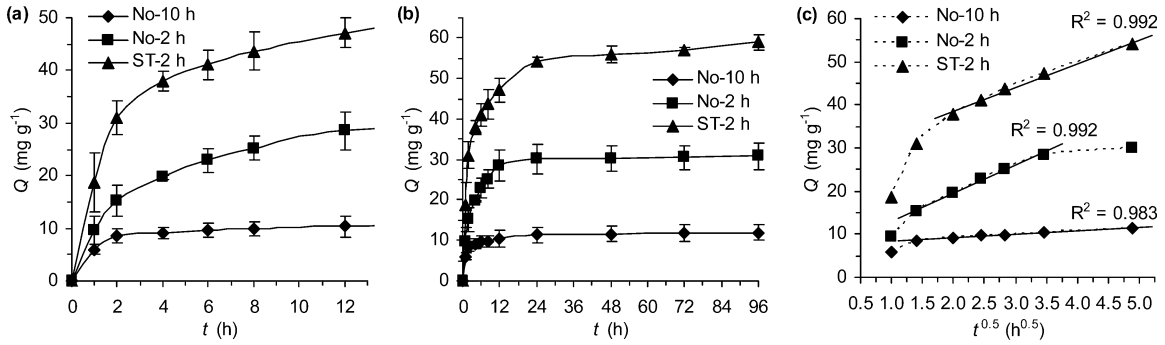

Figure 5. Profiles of cumulative release of ibuprofen (Q) from the TiO_2 networks against (a) time up to 12 h, (b) time through to 96 h, and (c) the square root of time (Higuchi model).

Supporting Information). This adsorption data, taken in conjunction with the SEM images in Figure 4, provides clear evidence that apatite will both nucleate and grow on a three-dimensional, structured, sol–gel anatase TiO_2 surface with low, moderate, or high initial specific surface areas (12.3, 48.9, or 110 m^2 g^{-1}, respectively).

Ibuprofen Adsorption and Release. With their bimodal porous structures and variable surface areas, TiO_2 networks prepared from a collagen template could serve as DDVs. Indeed, the large open spaces between the network fibers could assist in the dispersion of drug molecules in vivo, after egress from the mesoporous TiO_2 fibers. The three networks (No-10 h, No-2 h, and ST-2 h) cover a wide surface area range (see

Table 1). The anti-inflammatory drug ibuprofen was employed to test the efficacy of the TiO_2 networks as DDVs, through study of drug adsorption, release, and the effects on surface area and mesoporosity. A brief overview of the medicinal and chemical properties of ibuprofen, and consideration of other model drugs is provided in the Supporting Information. The ibuprofen molecule is approximately 1 × 0.6 nm^2—sufficiently small to fit within mesopores.[35,38,40,42] For drug delivery studies, ibuprofen is frequently dissolved in hexane at concentrations in the range of 30−40 mg mL^{-1}.[32,36−42,44,45] In this study the concentration was 30 mg mL^{-1}. Additionally, it should be noted that the drug loading/release results obtained were for nonfunctionalized TiO_2 networks. It is expected that greater control over both drug loading and release could be achieved by surface functionalization, as has been demonstrated by Vallet-Regí and co-workers on mesoporous SiO_2 and templated glass DDVs.[35,46]

Nitrogen sorption was used to examine the effect of ibuprofen storage on the surface area and porosity of ground TiO_2 networks. While there was no significant decrease in mesopore diameter—the pores were of ample diameter to host the drug molecules—both surface area and pore volume were reduced for all three drug-loaded networks (see Table 2).

Ibuprofen release behaviors, as studied by UV−visible spectroscopy, from the three TiO_2 networks over a 96 h period in PBS are shown in Figure 5a and b. For all networks there was an initial burst release of drug (No-10 h and No-2 h: t < 2 h; ST-2 h: t < 4 h) followed by a period of sustained release until equilibrium was reached (No-10 h and ST-2 h: 24 < t < 48 h; No-2 h: 12 < t < 24 h). The amount of drug released was greatest for ST-2 h, which had been solvothermally treated as a hybrid, with the release diminishing in turn for the two nontreated samples, No-2 h and No-10 h (see Table 2).

According to the Higuchi model, diffusion of drug molecules proceeded in a Fickian manner if a straight line resulted from the graphing of cumulative drug release against the square root of release time.[40] Linear plots were obtained for ibuprofen release from all TiO_2 networks (see Figure 5c), signifying that ibuprofen release from these structures follows a Fickian diffusion mechanism. The mechanism can be explained due to weak hydrogen bonding interaction between the carboxylic group of ibuprofen and the TiO_2 surface—the bonding force is insufficient to affect the drug release process.[35,40] Nonetheless, it should be recalled that unbound drug molecules diffused first from the TiO_2 networks, and in a non-Fickian way: a burst release. The Higuchi-modeled apparent onset and cessation of Fickian diffusion varied across the three networks (Figure 5c). For ST-2 h, which had a greater and more prolonged period of burst release, Fickian diffusion did not occur until t = 4 h. Contrastingly, the diffusion behavior ceased earlier for No-2 h at t = 12 h than for the other two scaffolds. No-2 h had the fastest ibuprofen diffusion rate. The long diffusion period of No-10 h (t = 2−24 h) may be ascribed to its low Higuchi dissolution constant. A lack of correlation between individual measured physical parameters and the Higuchi dissolution constant (Table 2) suggests that it is the interplay between the differences that influences the determined rate constant.

The decrease in surface area was due to adsorption of ibuprofen to the TiO_2 walls of the networks. Ibuprofen interacts with TiO_2 through hydrogen bonding between its carboxylic group and surface Ti−OH groups; any non-coordinated ibuprofen is hosted in the pore cavity.[35,40] Manzano and Vallet-Regí have utilized nitrogen sorption to investigate whether drug molecules are confined within the mesopores of a matrix (i.e., occupying the cavity space), or are merely on the outer surface. A decrease in pore volume was considered evidence of drug molecules partially filling the mesopores. Concurrently, surface area typically decreases due to host−guest interaction.[35] The mesopore volume for all three TiO_2 networks was reduced after ibuprofen incorporation, implying that ibuprofen had partly occupied the pore space (see Figure S7 in the Supporting Information), a finding supported by the diminished single-point pore volume (Table 2). Pore volume associated with larger mesopores (>15 nm) and macropores was similar both before and after ibuprofen loading (see Figure S7 in the Supporting Information), suggesting that nonadsorbed ibuprofen could only be hosted within the principal mesopore of the TiO_2 matrix, and that the ibuprofen molecule was too small to make a detectable difference to the pore volume of the larger pores.

Ibuprofen storage and release was influenced by surface area, and mesopore size and volume. Drug adsorption, as well as release, was higher for the solvothermally treated sample ST-2 h than the two untreated TiO_2 networks. Thus, for anatase TiO_2 networks, larger mesopore dimensions and greater surface area enabled more ibuprofen to be loaded. Judged against the literature,[32,36−45] the amount of ibuprofen adsorbed by the networks appears to be low. However, when drug storage was normalized against the preadsorption surface area (see the Supporting Information), the TiO_2 networks compared favorably with a variety of high surface area DDVs such as molecular sieves,[36−39] hollow spheres,[32,40] fibers,[41] zeolites,[42] and metal−organic frameworks[43−45] (see Table S1 in the Supporting Information).

This DDV data, when taken in context with both the open network morphology and the shown bioactivity, suggests that any structured, sol−gel anatase TiO_2 network of a range of surface areas (12.3−110 m^2 g^{-1}), could be effective materials for biomedical applications, including bone tissue engineering. Variable surface areas and mesopore dimensions enable control over the drug loading and release. Chemical bonding of the DDV to bone tissue at the bone defect site could be expected, with the biomineralization process being unaffected by the surface area of the DDV, at least for the surface areas studied here. Moreover, the open spaces between the mesoporous fibers of these TiO_2 networks are on the same scale as the smallest of the pores in bone.[46] These spaces between the fibers could aid in dispersing drug molecules in vivo, after they have diffused out of the TiO_2 fibers, as well as providing potential for the in-growth of surrounding tissues.

CONCLUSIONS

Type I collagen gel was demonstrated as an effective template for the synthesis of bimodal porous TiO_2 networks, with fibers possessed of walls up to 300 nm in thickness, and central hollows of 50−100 nm. Variations in the employment of solvothermal treatment and length of calcination time produced highly crystalline, anatase TiO_2 porous networks composed of mesoporous fibers with surface areas from 12.3 to 110 m^2 g^{-1} and mesopore diameters of 4.2, 5.3, and 8.8 nm. Solvothermal treatment produced the material with the highest surface area and largest mesopore diameter. In vitro bioactivity was demonstrated with the nucleation and growth of apatite, albeit almost exclusively on the outside of the scaffold, when placed in a simulated body fluid. Apatitic development was seemingly unaffected by differences in the substrate surface area. The

presence of apatite caused a drop in mesopore volume. The TiO_2 networks were capable of the adsorption and release of the drug ibuprofen. Higher loading and release rates were obtained for the networks with greater surface area and larger mesopore size. Drug storage occurred at both at the TiO_2 surface and within mesopores. Ibuprofen release was through a sustained diffusion mechanism (Fick's law) after an initial burst release. The TiO_2 networks compared well against literature drug delivery vehicles based on their surface area-normalized drug storage. Therefore, having exhibited both bioactivity and drug storage and release capability, TiO_2 porous networks could be proposed as a new class of material for biomedical applications.

■ ASSOCIATED CONTENT

Supporting Information

SEM images; TGA and DTA; nitrogen sorption isotherms and pore size distributions; EDS spectrum; a table of the preadsorption surface area normalized ibuprofen storage of various porous solids. Discussions on m-SBF, ibuprofen, other model drugs, and the comparison of drug storage capacity normalized against surface area. This material is available as a PDF free of charge via the Internet at http://pubs.acs.org.

■ AUTHOR INFORMATION

Corresponding Author

*E-mail: rcaruso@unimelb.edu.au.

Author Contributions

The manuscript was written through contributions of all authors.

Notes

The authors declare no competing financial interest.

■ ACKNOWLEDGMENTS

Devro Pty. Ltd. is thanked for providing the initial supplies of collagen for free. The Particulate Fluids Processing Centre, Electron Microscopy Unit at the Bio21 Institute, Electron Microscopy Facility in the School of Botany, and CSIRO are all thanked for instrument support. W.A.M. acknowledges The University of Melbourne for a Science Faculty Scholarship. CSIRO is acknowledged for the OCE Science Leader Scheme. R.A.C. acknowledges the Australian Research Council for an ARC Future Fellowship (FT0990583).

■ REFERENCES

(1) Deshpande, A. S.; Shchukin, D. G.; Ustinovich, E.; Antonietti, M.; Caruso, R. A. *Adv. Funct. Mater.* **2005**, *15*, 239−245.
(2) Chee Kimling, M.; Caruso, R. A. *J. Mater. Chem.* **2012**, *22*, 4073−4082.
(3) Caruso, R. A.; Antonietti, M. *Chem. Mater.* **2001**, *13*, 3272−3282.
(4) Zhou, J. F.; Zhou, M. F.; Caruso, R. A. *Langmuir* **2006**, *22*, 3332−3336.
(5) Eglin, D.; Mosser, G.; Giraud-Guille, M.-M.; Livage, J.; Coradin, T. *Soft Mater.* **2005**, *1*, 129−131.
(6) Cai, L.; Liao, X. P.; Shi, B. *Ind. Eng. Chem. Res.* **2010**, *49*, 3194−3199.
(7) Deng, D. H.; Tang, R.; Liao, X. P.; Shi, B. *Langmuir* **2008**, *24*, 368−370.
(8) Deng, D. H.; Wu, H.; Liao, X. P.; Shi, B. *Microporous Mesoporous Mater.* **2008**, *116*, 705−709.
(9) Deng, D. H.; Liao, X. P.; Liu, X.; Shi, B. *J. Mater. Res.* **2008**, *23*, 3263−3268.
(10) Ono, Y.; Kanekiyo, Y.; Inoue, K.; Hojo, J.; Nango, M.; Shinkai, S. *Chem. Lett.* **1999**, *28*, 475−476.
(11) Heinemann, S.; Heinemann, C.; Jäger, M.; Neunzehn, J.; Wiesmann, H. P.; Hanke, T. *ACS Appl. Mater. Interfaces* **2011**, *3*, 4323−4331.
(12) Wang, C.-C.; Ying, J. Y. *Chem. Mater.* **1999**, *11*, 3113−3120.
(13) Chen, X.; Mao, S. S. *Chem. Rev.* **2007**, *107*, 2891−2959.
(14) Brinker, C. J.; Scherer, G. W. *Sol−Gel Science: The Physics and Chemistry of Sol−Gel Processing*; Academic Press: San Diego, CA, 1990.
(15) Chen, D. H.; Cao, L.; Huang, F. Z.; Imperia, P.; Cheng, Y.-B.; Caruso, R. A. *J. Am. Chem. Soc.* **2010**, *132*, 4438−4444.
(16) Liu, C.-Z. *J. Bionic Eng. Suppl.* **2008**, 001−008.
(17) Baia, L.; Baia, M.; Danciu, V.; Albu, M. G.; Coşoveanu, V.; Iordăchescu, D.; Trandafir, V. *J. Optoelectron. Adv. Mater.* **2008**, *10*, 933−936.
(18) Thula, T. T.; Rodriguez, D. E.; Lee, M. H.; Pendi, L.; Podschun, J.; Gower, L. B. *Acta Biomater.* **2011**, *7*, 3158−3169.
(19) Góes, J. C.; Figueiró, S. D.; Oliveira, A. M.; Macedo, A. A. M.; Silva, C. C.; Ricardo, N. M. P. S.; Sombra, A. S. B. *Acta Biomater.* **2007**, *3*, 773−778.
(20) Al-Munajjed, A. A.; Plunkett, N. A.; Gleeson, J. P.; Weber, T.; Jungreuthmayer, C.; Levingstone, T.; Hammer, J.; O'Brien, F. J. *J. Biomed. Mater. Res., Part B* **2009**, *90B*, 584−591.
(21) Lickorish, D.; Ramshaw, J. A. M.; Werkmeister, J. A.; Glattauer, V.; Howlett, C. R. *J. Biomed. Mater. Res., Part A* **2004**, *68A*, 19−27.
(22) Wahl, D. A.; Czernuszk, J. T. *Eur. Cell. Mater.* **2006**, *11*, 43−56.
(23) Liao, X. P.; Shi, B. *Environ. Sci. Technol.* **2005**, *39*, 4628−4632.
(24) Maas, M.; Guo, P.; Keeney, M.; Yang, F.; Hsu, T. M.; Fuller, G. G.; Martin, C. R.; Zare, R. N. *Nano Lett.* **2011**, *11*, 1383−1388.
(25) Przybyla, D. E.; Chmielewski, J. *Biochemistry* **2010**, *49*, 4411−4419.
(26) Boki, K. In *Surface of Nanoparticles and Porous Materials*; Schwarz, J. A., Contescu, C. I., Eds.; Marcel Dekker: New York, 1999; pp 185−198.
(27) Holzwarth, J. M.; Ma, P. X. *J. Mater. Chem.* **2011**, *21*, 10243−10251.
(28) Hertz, A.; Bruce, I. J. *Nanomedicine* **2007**, *2*, 899−918.
(29) Bigi, A.; Boanini, E.; Panzavolta, S.; Roveri, N. *Biomacromolecules* **2000**, *1*, 752−756.
(30) Pei, A.-H.; Shen, Z.-W.; Yang, G.-S. *Mater. Lett.* **2007**, *61*, 2757−2760.
(31) Xia, W.; Grandfield, K.; Hoess, A.; Ballo, A.; Cai, Y.; Engqvist, H. *J. Biomed. Mater. Res., Part B* **2012**, *100B*, 82−93.
(32) Yao, L.-F.; Shi, Y.; Jin, S.-R.; Li, M.-J.; Zhang, L.-M. *Mater. Res. Bull.* **2010**, *45*, 1351−1356.
(33) Vallet-Regí, M.; Balas, F.; Arcos, D. *Angew. Chem., Int. Ed.* **2007**, *46*, 7548−7558.
(34) Fatouros, D. G.; Douroumis, D.; Nikolakis, V.; Ntais, S.; Moschovi, A. M.; Trivedi, V.; Khima, B.; Roldo, M.; Nazar, H.; Cox, P. A. *J. Mater. Chem.* **2011**, *21*, 7789−7794.
(35) Manzano, M.; Vallet-Regí, M. *J. Mater. Chem.* **2010**, *20*, 5593−5604.
(36) Horcajada, P.; Rámila, A.; Pérez-Pariente, J.; Vallet-Regí, M. *Microporous Mesoporous Mater.* **2004**, *68*, 105−109.
(37) Muñoz, B.; Rámila, A.; Pérez-Pariente, J.; Díaz, I.; Vallet-Regí, M. *Chem. Mater.* **2003**, *15*, 500−503.
(38) Vallet-Regí, M.; Rámila, A.; del Real, R. P.; Pérez-Pariente, J. *Chem. Mater.* **2001**, *13*, 308−311.
(39) Zhao, F. C.; Li, G.; Wang, X. X.; Sun, D. W.; Jin, C. Z. *J. Porous Mater.* **2010**, *17*, 629−634.
(40) Zhu, Y. F.; Shi, J. L.; Shen, W. H.; Chen, H. R.; Dong, X. P.; Ruan, M. L. *Nanotechnology* **2005**, *16*, 2633−2638.
(41) Ma, Z.; Ji, H.; Teng, Y.; Dong, G.; Tan, D.; Guan, M.; Zhou, J.; Xie, J.; Qiu, J.; Zhang, M. *J. Mater. Chem.* **2011**, *21*, 9595−9602.
(42) Horcajada, P.; Márquez-Alvarez, C.; Rámila, A.; Pérez-Pariente, J.; Vallet-Regí, M. *Solid State Sci.* **2006**, *8*, 1459−1465.
(43) Horcajada, P.; Ruxandra, G.; Baati, T.; Allan, P. K.; Maurin, G.; Couvreur, P.; Férey, G.; Morris, R. E.; Serre, C. *Chem. Rev.* **2012**, *112*, 1232−1268.

(44) Horcajada, P.; Serre, C.; Maurin, G.; Ramsahye, N. A.; Balas, F.; Vallet-Regí, M.; Sebban, M.; Taulelle, F.; Férey, G. *J. Am. Chem. Soc.* **2008**, *130*, 6774−6780.
(45) Horcajada, P.; Serre, C.; Vallet-Regí, M.; Sebban, M.; Taulelle, F.; Férey, G. *Angew. Chem., Int. Ed.* **2006**, *45*, 5974−5978.
(46) Vallet-Regí, M.; Izquierdo-Barba, I.; Colilla, M. *Philos. Trans. R. Soc. London, Ser. A* **2012**, *370*, 1400−1421.
(47) Gertler, G.; Fleminger, G.; Rapaport, H. *Langmuir* **2010**, *26*, 6457−6463.
(48) Qin, Y.; Sun, L.; Li, X.; Cao, Q.; Wang, H.; Tang, X.; Ye, L. *J. Mater. Chem.* **2011**, *21*, 18003−18010.
(49) Peng, L.; Mendelsohn, A. D.; LaTempa, T. J.; Yoriya, S.; Grimes, C. A.; Desai, T. A. *Nano Lett.* **2009**, *9*, 1932−1936.
(50) Li, Q.; Wang, X.; Lu, X.; Tian, H.; Jiang, H.; Lv, G.; Guo, D.; Wu, C.; Chen, B. *Biomaterials* **2009**, *30*, 4708−4715.
(51) Bjursten, L. M.; Rasmusson, L.; Oh, S.; Smith, G. C.; Brammer, K. S.; Jin, S. *J. Biomed. Mater. Res., Part A* **2010**, *92A*, 1218−1224.
(52) Peltola, T.; Pätsi, M.; Rahiala, H.; Kangasniemi, I.; Yli-Urpo, A. *J. Biomed. Mater. Res.* **1998**, *41*, 504−510.
(53) Xia, W.; Lindahl, C.; Lausmaa, J.; Borchardt, P.; Ballo, A.; Thomsen, P.; Engqvist, H. *Acta Biomater.* **2010**, *6*, 1591−1600.
(54) Sampathkumaran, U.; De Guire, M. R.; Wang, R. *Adv. Eng. Mater.* **2001**, *3*, 401−405.
(55) Gunawidjaja, P. N.; Lo, A. Y. H.; Izquierdo-Barba, I.; García, A.; Arcos, D.; Stevensson, B.; Grins, J.; Vallet-Regí, M.; Edén, M. *J. Phys. Chem. C* **2010**, *114*, 19345−19356.
(56) Kim, H.-M. *Curr. Opin. Solid State Mater. Sci.* **2003**, *7*, 289−299.
(57) Kokubo, T. *Thermochim. Acta* **1996**, *280/281*, 479−490.
(58) Kokubo, T. *Mater. Sci. Eng., C* **2005**, *25*, 97−104.
(59) Kokubo, T.; Kim, H. M.; Kawashita, M. *Biomaterials* **2003**, *24*, 2161−2175.
(60) Kokubo, T.; Takadama, H. *Biomaterials* **2006**, *27*, 2907−2915.
(61) Kokubo, T.; Kim, H. M.; Kawashita, M.; Nakamura, T. *J. Mater. Sci.−Mater. Med.* **2004**, *15*, 99−107.
(62) Oyane, A.; Onuma, K.; Ito, A.; Kim, H. M.; Kokubo, T.; Nakamura, T. *J. Biomed. Mater. Res. Part A* **2003**, *64A*, 339−348.
(63) Dorozhkin, S. V.; Dorozhkina, E. I.; Epple, M. *Cryst. Growth Des.* **2004**, *4*, 389−395.
(64) Zhang, L.-J.; Feng, X.-S.; Liu, H.-G.; Qian, D.-J.; Zhang, L.; Yu, X.-L.; Cui, F.-Z. *Mater. Lett.* **2004**, *58*, 719−722.
(65) Ngo, P.; Ramalingam, R.; Phillips, J. A.; Furuta, G. T. In *Cell−Cell Interactions: Methods and Protocols*; Colgan, S. P., Ed.; Humana Press: Totowa, NJ, 2006; pp 103−109.
(66) Lowell, S.; Shields, J. E.; Thomas, M. A.; Thommes, M. *Characterization of Porous Solids and Powders: Surface Area, Pore Size, and Density*; Kluwer Academic Publishers: Dordrecht, The Netherlands, 2004.
(67) Jalota, S.; Bhaduri, S. B.; Tas, A. C. *J. Mater. Sci.−Mater. Med.* **2006**, *17*, 697−707.
(68) Tas, A. C.; Bhaduri, S. B. *J. Mater. Res.* **2004**, *19*, 2742−2749.